Theoretical Chemistry Accounts (2020) 139:125
https://doi.org/10.1007/s00214-020-02631-x

REGULAR ARTICLE

Quantitative assessment of intramolecular hydrogen bonds in neutral histidine

Seth F. Yannacone[1] · Daniel Sethio[2] · Elfi Kraka[1]

Received: 10 March 2020 / Accepted: 8 June 2020

Abstract
Experimentalists recently characterized the difficulty in isolating gaseous histidine in its neutral form. To understand the factors which stabilize neutral histidine, the intrinsic nature of the intramolecular hydrogen bonding networks in the four most stable histidine conformers was investigated via density functional theory combined with the local vibrational mode analysis originally introduced by Konkoli and Cremer, quantum theory of atoms in molecules, non-covalent interaction analysis, and natural bond orbital population analysis. Our results show a positive correlation between intramolecular hydrogen bond strength and structural stability, where the presence of the O−H ⋯ N_α bond type is a major factor.

Keywords Histidine · Hydrogen bonding · Local vibrational mode analysis · NBO analysis · QTAIM analysis · DLPNO-CCSD(T)

1 Introduction

Histidine (HIS) is one of the twenty essential amino acids relevant to biological organisms [1] and involves innate processes such as tissue growth and muscle repair [2, 3]. HIS consists of an imidazole (Im) ring and a side chain with branched amine (NH_2) and carboxyl (CO_2H) groups, which can switch from neutral (R−NH_2 and R−CO_2H) to zwitterionic forms (R−NH_3^+ and R−CO_2^-), depending on physiological conditions such as pH and temperature [4]. Hence, HIS acts as both proton acceptor and donor in biochemical reactions [5]. Additionally, Im-N (N_δ) can be deprotonated (ε tautomer) or protonated (δ tautomer), allowing for inter- and intramolecular hydrogen bonds (HBs). Functionality in HIS relates to its three-dimension conformation [6], which in turn depends on non-covalent interactions (NCIs) [7]. Experimental and theoretical studies suggest that the conformational preference of HIS is primarily influenced by the stabilizing presence of intramolecular hydrogen bonds (IMHBs) [8, 9], but to our best knowledge this has not been quantified.

HIS exists predominantly as a zwitterion, where it gains extra stabilization energy through interactions with polar environments [10]. The zwitterion exists over a wide pH range in liquid and solid phases [11]. Due to its high melting point, low vapor pressure, and thermal instability, neutral HIS has proven difficult to isolate and experimentally characterize. εII_a (Fig. 1) is the most stable/common in nature [12, 13] and was recently isolated and characterized in the gas phase for the first time using laser ablation techniques [14], which has opened the door for research aimed at better understanding the factors involved in stabilizing this neutral form.

In this work, we present for the first time a quantitative analysis of IMHB strength in the four most stable

"Festschrift in honor of Prof. Fernando R. Ornellas" Guest Edited by Adélia Justino Aguiar Aquino, Antonio Gustavo Sampaio de Oliveira Filho & Francisco Bolivar Correto Machado.

Electronic supplementary material The online version of this article (https://doi.org/10.1007/s00214-020-02631-x) contains supplementary material, which is available to authorized users.

✉ Elfi Kraka
ekraka@smu.edu

Seth F. Yannacone
syannacone@smu.edu

Daniel Sethio
sethio.daniel@kemi.uu.se

[1] Computational and Theoretical Chemistry Group (CATCO), Department of Chemistry, Southern Methodist University, 3215 Daniel Avenue, Dallas, TX 75275-0314, USA

[2] Department of Chemistry, Uppsala University, Box 576, 75123 Uppsala, Sweden

Published online: 27 June 2020

HIS conformers (εII_a, εII_b, δII_a, and δI_a) with the aim of answering the following questions:

(i) Which theoretical (DFT) method gives the best description of IMHBs?
(ii) Which types of IMHBs are possible in neutral HIS?
(iii) How strong are the IMHBs in neutral HIS?
(iv) What factors stabilize neutral HIS?
(v) Why is εII_a more stable than δII_a? What factors stabilize εII_a?

2 Computational methods

The major reason why IMHBs in HIS have not been quantified so far has been the lack of a reliable intrinsic bond strength measure. Detailed information on the electronic structure of a molecule and its chemical bonds is encoded in the molecular normal vibrational modes. However, normal vibrational modes are generally delocalized in polyatomic molecules because of electronic and mass coupling. [15–18] Therefore, the corresponding normal mode frequencies and force constants are not suitable bond strength descriptors [19]. Konkoli, Cremer, and co-workers provided a solution to this problem utilizing a mass-decoupled analogue of Wilson's equation of vibrational spectroscopy leading to local vibrational modes (LVMs) that are free from any mode–mode coupling [20–24]. Each local mode is associated with an internal coordinate q_n (e.g., bond length r) which drives the local vibration and a corresponding local mode frequency ω^a and local mode force constant k^a. Zou and co-workers demonstrated that there is a one-to-one relationship between the local and normal vibrational modes, that can be verified by an adiabatic connection scheme (ACS), providing the physical fundament for the LMVs.[25] Zou and Cremer further proved that the local stretching force constant k^a is directly related to the intrinsic strength of a bond, which qualifies k^a as unique quantitative bond strength measure based on vibrational spectroscopy.[26] So far, the local mode analysis has been successfully applied to characterize covalent bonds [26–32] and weak chemical interactions such as halogen [33–36], chalcogen [37–39], pnicogen [40–42], and tetrel interactions [43] as well as intra- and intermolecular hydrogen bonding in various forms and systems.[44–50]

To simplify the comparison of local stretching force constants k^a, we generally convert k^a values into bond strength orders (BSO n) most chemists are more acquainted with [28, 29, 44, 51] via a generalized Badger rule [27, 52] which states that the strength of a bond correlates with the local force constant in the form of a power relationship:

$$\text{BSO } n = a(k^a)^b. \tag{1}$$

The constants a and b can be determined from 2 reference molecules with defined BSO n and known k^a values and the assumption that $k^a = 0$ corresponds to $n = 0$. In this work, we used as references HF (BSO $n = 1$ and $k^a = 9.350$ mdyn/Å) and HF_2^- (BSO $n = 0.5$ and $k^a = 0.852$ mdyn/Å). This led to $a = 0.524$ and $b = 0.289$. We determined the covalent character of the IMHBs via the Cremer–Kraka criterion [53, 54] for covalent bonding which is based on the local energy density $H(\mathbf{r})$

$$H(\mathbf{r}) = G(\mathbf{r}) + V(\mathbf{r}), \tag{2}$$

where $G(\mathbf{r})$ is the kinetic energy density (positive, destabilizing) and $V(\mathbf{r})$ is the potential energy density (negative, stabilizing). Taken at the bond critical point $\mathbf{r}_b$ of the electron density $\rho(\mathbf{r})$ [55, 56] between two bonded atoms, $H(\mathbf{r}_b) < 0$ points to a covalent interaction, while $H(\mathbf{r}_b) > 0$ indicates an electrostatic interaction.

To find a practical and reliable computational method for describing weak IMHBs, the influence of dispersion corrections was evaluated using (i) the semiclassical C_6-based schemes of Grimme's D2 [57], D3 [58], and D3(BJ) [59] dispersion corrections in combination with B3LYP [60] and (ii) the range-separated, dispersion-corrected ωB97X-D [61] functional. We also compared Pople's 6-311++G(d,p) [62] triple-ζ augmented basis set with polarization and diffuse functions with Dunning's aug-cc-pVTZ [63] correlation-consistent triple-ζ basis set of the same quality and features [64]. B3LYP-D3(BJ)/aug-cc-pVTZ turned out to be the most accurate level of theory for this work. The aug-cc-pVTZ basis set contains higher-quality polarization and diffuse functions compared to 6-311++G(d,p), and the B3LYP-D3(BJ) functional/dispersion correction combination provided a more accurate description of IMHBs compared to ωB97X-D (See Supporting Information).

A dual-level strategy was utilized, where geometry optimizations and frequencies were calculated at the B3LYP-D3(BJ)/aug-cc-pVTZ level of theory. Single-point energies were then calculated via the domain local pair natural orbital coupled cluster theory with singles, doubles, and perturbative triples (DLPNO-CCSD(T)) method [65, 66] and aug-cc-pVTZ basis set.

DFT calculations were performed using Gaussian09 version D.01 [67]. Geometry optimizations and vibrational frequencies were calculated with an ultra-fine integration grid and tight convergence criteria for forces and displacement. DLPNO-CCSD(T) single-point energies were calculated using ORCA [68]. Charge distribution and local charges were calculated using NBO6 [69, 70]. LVM frequencies (ω^a) and k^a were calculated using COLOGNE2017 [71]. Electron density ($\rho(\mathbf{r}_b)$) [72] and $H(\mathbf{r}_b)$, where $\mathbf{r}_b$ is a bond

critical point, were calculated using AIMAll [73]. Structural models were made with UCSF Chimera [74]. NCI plots were made with 'isosurface NCIPLOT' in Jmol [75, 76]. Standard gradient cutoff of $s = 0.5$ a.u. (s: the reduced density gradient) with color scale $-0.04 < \rho < 0.04$ au was utilized [75]. LVM, AIMALL, and NCI plots all support the IMHBs discussed in the following section. To provide further support for this work, the density-dependent density overlap regions indicator (DORI) analysis was utilized (see Supporting Information) [77].

3 Results and discussion

Table 1 summarizes relative (with respect to εII_a) electronic plus zero-point energies (ΔE), electronic plus thermal enthalpies (ΔH), electronic plus thermal free energies (ΔG), CCSD(T) ΔE corrections (ΔE_{corr}), IMHB distances (r), local mode force constants (k^a), local mode frequencies (ω^a), bond strength order (BSO n), electron density ($\rho(\mathbf{r}_b)$), local energy density ($H(\mathbf{r}_b)$), and bond degree (BD: $H(\mathbf{r}_b)/\rho(\mathbf{r}_b)$) [78]. Calculated molecular geometries, selected NBO atomic charges, IMHBs (green dashed bonds), bond distances (r) reported in Å, and NCI isosurfaces (bottom row) are shown in Fig. 1. For the NCI plots, blue isosurfaces represent strongly attractive interactions, green/yellow surfaces indicate weakly attractive interactions, and orange/red surfaces point to repulsive interactions.

In Fig. 2, local stretching force constants k^a of IMHBs are plotted with respect to IMHB distance r. Figure 3 shows a power relationship between BSO n and k^a of the 12 IMHBs in this work. In Fig. 4, BSO n is plotted with respect to local energy density at the BCP ($H(\mathbf{r}_b)$), where the vertical dashed line at $H(\mathbf{r}_b) = 0$ separates the covalent ($H(\mathbf{r}_b) < 0$) and electrostatic ($H(\mathbf{r}_b) \geq 0$) regions according to the Cremer–Kraka criterion. Figure 5 reveals a correlation between BSO n and $\rho(\mathbf{r}_b)$, where increased electronic density correlates with increased IMHB strength. Figure 6 shows the sum of IMHB k^a values for each HIS conformer plotted with respect to ΔE_{corr}.

3.1 Intrinsic strength of IMHBs

Each conformer has a unique network of IMHBS, together comprising eight different IMHB types:

1. N_α–H···N_δ (εII_a, εII_b), donor/acceptor = NH_2/Im-N, [purple circles]
2. N_δ–H···N_α (δI_a), donor/acceptor = Im-NH/ NH_2, [orange diamond]
3. N_α–H···O (δI_a), donor/acceptor = NH_2/carbonyl-O, [brown hexagon]
4. C_β–H···O=C (εII_a, δII_a), donor/acceptor = CH_2/carbonyl-O, [red squares]
5. C_β–H···OH (δI_a), donor/acceptor = CH_2/OH, [red squares]
6. O–H···N_α (εII_a, εII_b, δII_a), donor/acceptor = OH/NH_2, [blue triangles]
7. N_δ–H···O (δII_a), donor/acceptor = Im-NH/carbonyl-O, [blue pentagon]
8. N_α – H···C_δ (δII_a), donor/acceptor = NH_2/Im-C, [green triangle]

Table 1 Relative electronic plus zero-point energies (ΔE), electronic plus thermal enthalpies (ΔH), electronic plus thermal free energies (ΔG), CCSD(T) ΔE corrections (ΔE_{corr}), IMHB distances (r), local stretching force constants (k^a), local mode frequencies (ω^a), bond strength order (BSO n), electron density ($\rho(\mathbf{r}_b)$), local energy density ($H(\mathbf{r}_b)$), and bond degree (BD = $H(\mathbf{r}_b)/\rho(\mathbf{r}_b)$)

Conformer	ΔE	ΔH	ΔG	ΔE_{corr}	Parameter	r	k^a	ω^a	BSO n	$\rho(\mathbf{r}_b)$	$H(\mathbf{r}_b)$	BD
εII_a	0.00	0.00	0.00	0.00	N_α–H···N_δ	2.176	0.116	457	0.281	0.124	0.012	0.096
–	–	–	–	–	O–H···N_α	1.861	0.277	707	0.362	0.275	− 0.031	− 0.114
–	–	–	–	–	O···H–C_βH	2.621	0.142	504	0.298	0.166	0.010	0.059
εII_b	1.22	1.25	1.23	1.44	N_α–H···N_δ	2.163	0.132	489	0.292	0.129	0.012	0.093
–	–	–	–	–	O–H···N_α	1.892	0.250	672	0.351	0.257	− 0.022	− 0.084
δII_a	0.52	0.48	0.83	0.49	O–H···N_α	1.906	0.244	663	0.349	0.249	− 0.016	− 0.065
–	–	–	–	–	N_δ–H···O	2.281	0.074	365	0.247	0.087	0.017	0.198
–	–	–	–	–	C_β – H···O=C	2.635	0.138	498	0.296	0.156	0.010	0.067
–	–	–	–	–	N_α – H···C_δ	2.861	0.056	321	0.228	0.068	0.006	0.086
δI_a	2.89	3.05	2.81	2.72	N_δ – H···N_α	2.275	0.102	428	0.271	0.117	0.015	0.128
–	–	–	–	–	HO···H–C_βH	2.611	0.134	489	0.293	0.177	0.007	0.039
–	–	–	–	–	N_α–H···O	2.267	0.108	441	0.275	0.128	0.015	0.118

Calculated at B3LYP-D3(BJ)/aug-cc-pVTZ//DLPNO-CCSD(T)/aug-cc-pVTZ levels of theory. IMHBs are denoted under 'Parameter' as dotted bonds. Thermochemical data are reported as relative to εII_a in kcal/mol, r in Å, k^a in mdyn/Å, ω^a in cm^{-1}, $\rho(\mathbf{r}_b)$ in e/$Å^3$, $H(\mathbf{r}_b)$ in Hartree/$Å^3$, and BD in Hartree/e

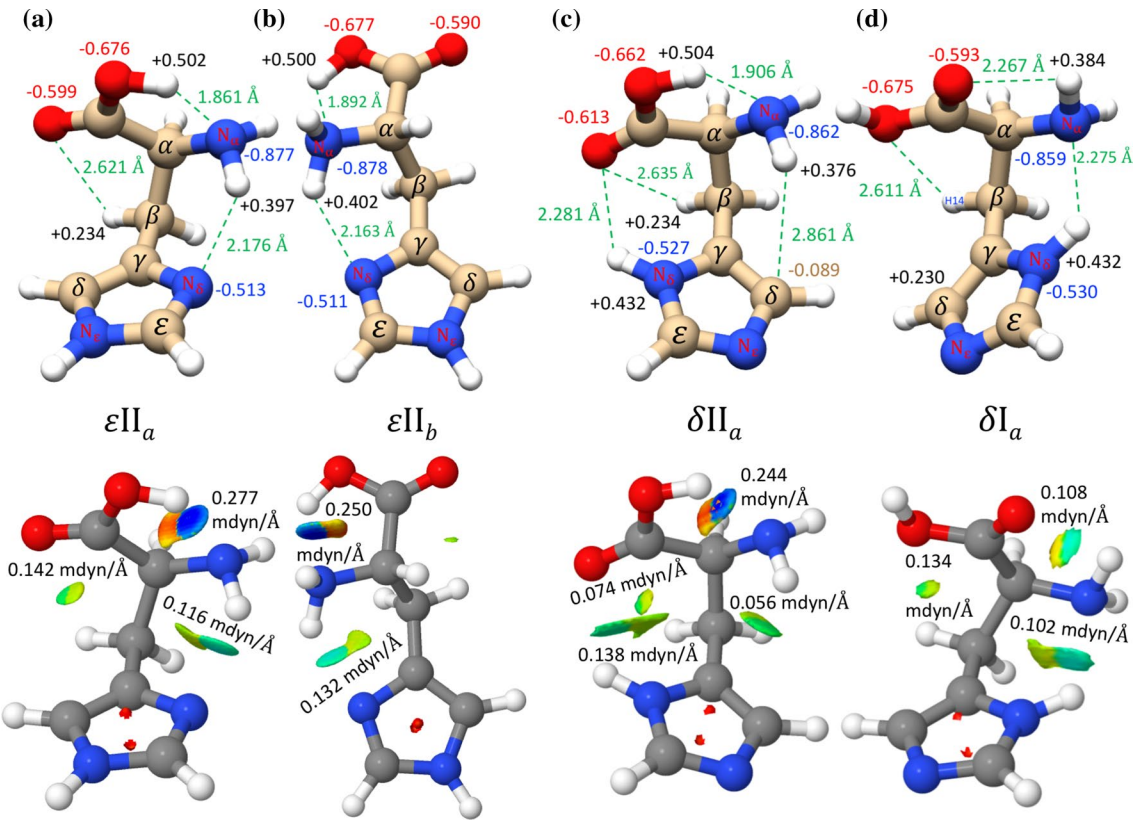

Fig. 1 (top) Structures of εII_a, εII_b, δII_a, and δI_a showing selected NBO charges and IMHBs as green dashed bonds. H, N, O, and C charges are shown in black, blue, red, and gold, respectively. (bottom) NCI plots showing isosurfaces and local vibrational force constants (k^a) for each IMHB. Blue surfaces represent strongly attractive, green/yellow surfaces are weakly attractive, and orange/red surfaces are repulsive

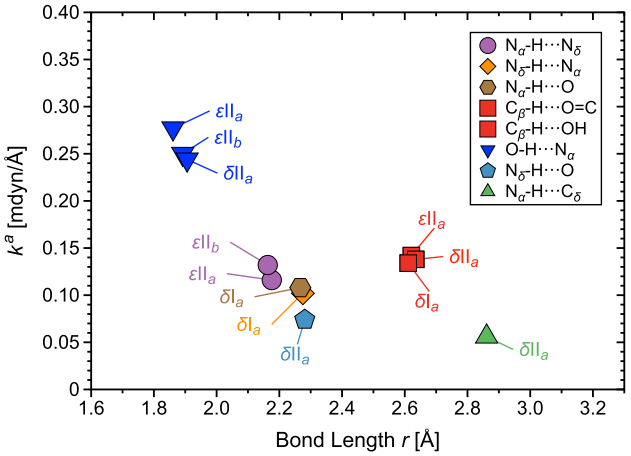

Fig. 2 Local stretching force constant (k^a) plotted with respect to IMHB length

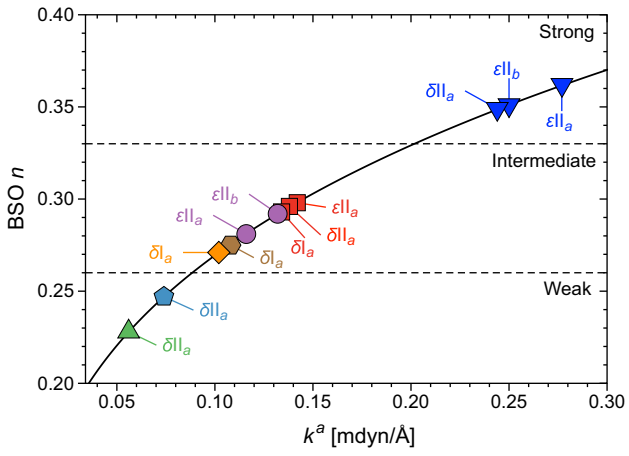

Fig. 3 Power relationship between bond strength order (BSO n) and local stretching force constants (k^a) of IMHBs in εII_a, εII_b, δII_a, and δI_a

Note: donor/acceptor refers to HB donor/HB acceptor, [color shape] indicates plot points in Figs. 2, 3, 5 and 6, N_α = amino-N, N_δ = Im-N, C_δ = Im−C, and C_β = aliphatic-C.

Despite different physical location and pairs, IMHB type 1, type 2, and type 3 have comparable bond distances and strengths. The nature of IMHB type 1, type 2, and

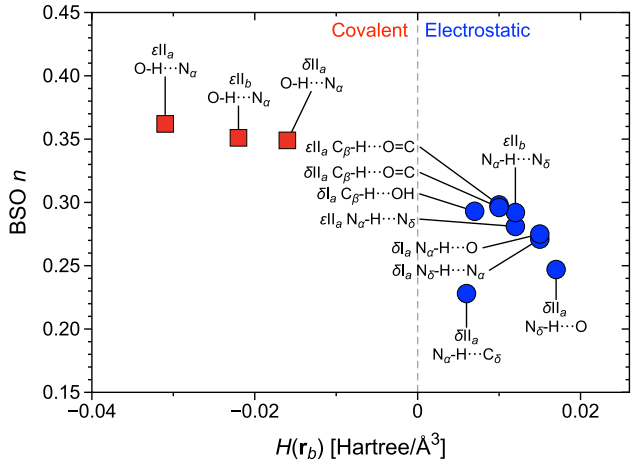

Fig. 4 Bond strength order (BSO n) plotted with respect to local energy density at the bond critical point ($H(\mathbf{r}_b)$)

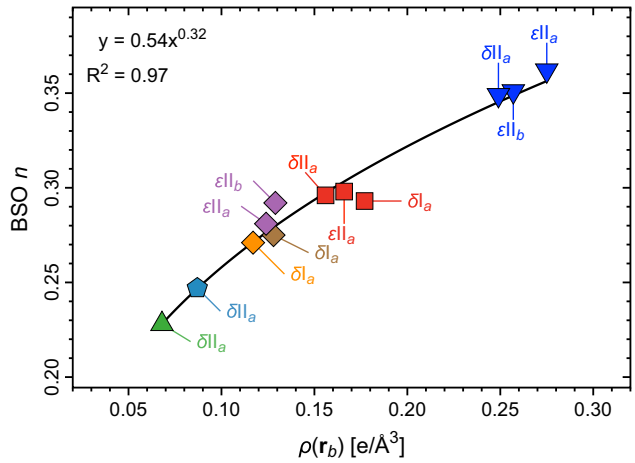

Fig. 5 Bond strength order (BSO n) plotted with respect to electron density at the bond critical point ($\rho(\mathbf{r}_b)$)

type 3 is electrostatic. IMHB type 1 is found in εII_a and εII_b, where N_α–H···N_δ found in εII_a is longer and weaker than the one found in εII_b. Type 2 and type 3 are uniquely found in δI_a.

Type 4 and type 5 are electrostatic in nature. Type 4 having a carbonyl-O as a HB acceptor is found in εII_a and δII_a, whereas type 5 having a hydroxyl-O as a HB acceptor is uniquely found in δI_a. The C_β–H acts as a HB donor on the both types. Both types are longer than types 1–3 yet slightly stronger by ca. 0.024 mdyn/Å. IMHB type 5 are found to be 'intermediates' in terms of bond strength as illustrated in Fig. 3 ($0.260 < \mathrm{BSO}n < 0.330$).

IMHB type 6 is found in εII_a, εII_b, and δII_a. Type 6 is the shortest and strongest HB studied in this work. The local stretching force constant k^a values of type 6 are 79.35% larger than other IMHB types. The IMHB type 6 is covalent

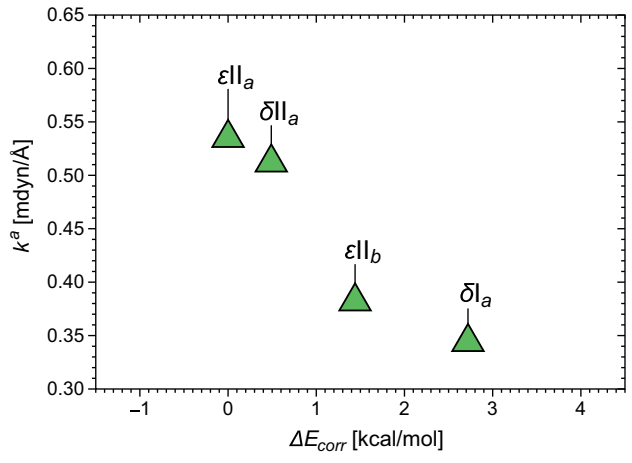

Fig. 6 Sum of local stretching force constants (k^a) plotted with respect to relative (with respect to εII_a) CCSD(T) correction to DFT electronic plus zero-point energy (ΔE_{corr})

in nature as shown in Fig. 4. The IMHB type 6 links CO_2H group to NH_2 group.

As a result of poor HB acceptor and poor HB donor, these types are the longest and weakest IMHB studied in this work. Types 7–8 are on average 63.16% weaker than other types. IMHB type 7 and type 8 are found uniquely in δII_a. Though it is rarely discussed, the existence of IMHB type 8 has been verified experimentally using X-ray crystallography, and in computational reports [79].

3.2 IMHB networks in each conformer

εII_a contains a three-IMHB network: $N_\alpha - H\cdots N_\delta$ (type 1), $C_\beta - H\cdots O = C$ (type 4), and $O - H\cdots N_\alpha$ (type 6). None of these interactions are unique to εII_a, but the combination is unique. This network links NH_2 to CO_2H, NH_2 to Im, and CO_2H to the C-backbone. $O - H\cdots N_\alpha$ ($k^a = 0.277$ mdyn/Å, BSO $n = 0.362$) is the strongest IMHB of εII_a (also of the four conformers), followed by $C_\beta - H\cdots O = C$ ($k^a = 0.142$ mdyn/Å, BSO $n = 0.298$), then $N_\alpha - H\cdots N_\delta$ ($k^a = 0.116$ mdyn/Å, BSO $n = 0.281$). Force constants of the three IMHBs sum to $k^a_{\varepsilon II_a} = 0.535$ mdyn/Å, the largest value compared to εII_b (0.382 mdyn/Å), δII_a (0.512 mdyn/Å), and δI_a (0.344 mdyn/Å). H···N_δ is 2.176 Å in length with Δq of 0.910 e. H···N_α is significantly shorter ($r = 1.861$ Å) and more polar ($\Delta q = 1.379$ e) due to the close proximity of NH_2 and CO_2H and the quality of the donor (OH). The third IMHB of εII_a ($C_\beta - H\cdots O = C$) is the longest and least polar of the three interactions ($r = 2.621$ Å, $\Delta q = 0.833$ e). This IMHB type, though often neglected in the HB conversation [80], is well characterized [81] and plays an important role in the structures of proteins, amino acids, and crystals [82–84].

εII_b, the R-enantiomer of εII_a, has two IMHBS: $N_\alpha - H\cdots N_\delta$ (type 1) and $O - H\cdots N_\alpha$ (type 6) with $r = 2.163, 1.892$ Å and $\Delta q = 0.913, 1.378$ e, respectively. Once again, neither type is unique to εII_b, but the combination is unique. Analogous to εII_a, NCI plots show $H\cdots N_\delta$ being weakly attractive and $H\cdots N_\alpha$ being strongly attractive. A tiny isosurface is seen between O and the $H - C_\beta$, but $C_\beta H\cdots O$ is 0.104 Å longer than that of $C_\beta - H\cdots O = C$ in εII_a and LVM/AIMALL calculations do not support a bond. In terms of k^a, $H\cdots N_\delta$ is stronger (+0.016 mdyn/Å) and $H\cdots N_\alpha$ is weaker (−0.027 mdyn/Å) than respective counterparts in εII_a (Fig. 2). BSO n values for $H\cdots N_\delta$ and $H\cdots N_\alpha$ are 0.292 and 0.351, respectively. $H\cdots N_\alpha$ is characterized as a covalent IMHB, with $\rho(\mathbf{r}_b) = 0.257$ e/Å^3 and $H(\mathbf{r}_b) = -0.022$ Hartree/Å^3, whereas $H\cdots N_\delta$ is electrostatic in nature ($\rho(\mathbf{r}_b) = 0.129$ e/Å^3, $H(\mathbf{r}_b) = 0.012$ Hartree/Å^3).

δII_a is an N-tautomer of εII_a with its Im ring flipped 179.14° and is the only conformer with four IMHBS: $C_\beta - H\cdots O{=}C$ (type 4), $O - H\cdots N_\alpha$ (type 6), $N_\delta - H\cdots O$ (type 7), and $N_\alpha - H\cdots C_\delta$ (type 8) with $r = 2.635, 1.906, 2.281, 2.861$ Å and $\Delta q = 0.847, 1.366, 1.045, 0.465$ e, respectively. The NCI plot confirms that $O - H\cdots N_\alpha$ is a strongly attractive interaction, while the other three IMHBs are all weakly attractive. $N_\delta - H\cdots O$ and $N_\alpha - H\cdots C_\delta$ are unique to δII_a as the only IMHBs with donor/acceptor combinations being $H - N_\delta$/carbonyl-O and $H - N_\alpha/C_\delta$, respectively. These two IMHBs are the only interactions with $k^a < 0.100$ mdyn/Å and BSO $n < 0.250$. $O - H\cdots N_\alpha$ is the only strong and covalent ($H(\mathbf{r}_b) = -0.016$ Hartree/Å^3) IMHB out of the four. εII_a is more stable than δII_a because: (i) $O - H\cdots N_\alpha$ and $O\cdots H - C_\beta H$ are stronger in εII_a, and (ii) the intermediately strong $N_\delta\cdots H - N_\alpha H$ in εII_a is replaced by the weak $N_\alpha - H\cdots C_\delta$ in δII_a.

δI_a is another tautomer of εII_a, with CO_2H and NH_2 rotated ≈ 180° about their C-C and C-N bond axes, respectively. This is the only conformer without the type 6 IMHB. Each IMHB in this case is technically unique to δI_a: $N_\delta - H\cdots N_\alpha$ (type 2), $N_\alpha - H\cdots O$ (type 3), and $C_\beta - H\cdots OH$ (type 5). However, as previously mentioned, type 4 and type 5 are highly similar. δI_a is also unique in that it does not have any IMHBs < 2.000 Å in length, the NCI plot in Fig. 1 indicates no strongly attractive interactions, and all three IMHBs are weak electrostatic interactions ($k^a < 0.200$ mdyn/Å, BSO $n < 0.300$, $H(\mathbf{r}_b) > 0.000$ Hartree/Å^3, $\rho(\mathbf{r}_b) < 0.200$ e/Å^3). $C_\beta - H\cdots OH$ is 2.611 Å in length and has a $O\cdots H\Delta q = 0.905$ e, $N_\alpha - H\cdots O$ is 2.267 Å in length with $O\cdots H\Delta q$ of 0.977 e, and $N_\delta - H\cdots N_\alpha$ is 2.275 Å in length with $N\cdots H\Delta q$ of 1.291 e. $C_\beta - H\cdots OH$ is the strongest IMHB in δI_a ($k^a = 0.134$ mdyn/Å, BSO $n = 0.293$), followed by $N_\alpha - H\cdots O$ ($k^a = 0.108$ mdyn/Å, BSO $n = 0.275$) and $N_\delta - H\cdots N_\alpha$ ($k^a = 0.102$ mdyn/Å, BSO $n = 0.271$). The trend in $\rho(\mathbf{r}_b)$ is similar to $H(\mathbf{r}_b)$, where the strongest IMHB, $C_\beta - H\cdots OH$, has the largest $\rho(\mathbf{r}_b)$ value (0.177 e/Å^3), but $N_\alpha - H\cdots O$ has slightly larger $\rho(\mathbf{r}_b)$ than $N_\delta - H\cdots N_\alpha$: 0.128 and 0.117 e/Å^3, respectively.

3.3 Relationship between intrinsic IMHB strength and relative stability

εII_a is the most thermochemically stable conformer by 0.49, 1.44, and 2.72 kcal/mol compared to δII_a, εII_b, and δI_a, respectively, in accord with previous studies [12–14]. The small ΔE values between the four conformers (< 2.72 kcal/mol) are in agreement with results from Kovačević et al. [85], and the 0.49 kcal/mol difference between the two most stable conformers, εII_a and δII_a, is near the 0.60 kcal/mol value previously reported by Huang et al [12]. In terms of cumulative IMHB force constants of each conformer: $\varepsilon II_a > \delta II_a > \varepsilon II_b > \delta I_a$, which matches the trend in ΔE and supports IMHB strength being a primary factor in the conformational stability of HIS.

$O - H\cdots N_\alpha$ is present in εII_a, εII_b, and δII_a but not in δI_a. Instead, $N_\alpha - H\cdots O$ links CO_2H to NH_2 in δI_a. The important difference between these two interactions is the donor/acceptor roles are reversed. The result being $N_\alpha - H\cdots O$ is drastically weaker ($k^a = 0.108$ mdyn/Å) and longer ($r = 2.267$ Å) than $O - H\cdots N_\alpha$ by ≈ 0.150 mdyn/Å and ≈ 0.380 Å. Consequently, absence of $O - H\cdots N_\alpha$ corresponds with δI_a being the least stable conformer. In addition, εII_a has the strongest type 6 IMHB with k^a more than 10% larger than in εII_b and δII_a.

Despite having only two IMHBs, εII_b is the third most stable HIS conformer, whereas δII_a has four IMHBs and is the second most stable. The most stable and least stable conformers each have three IMHBs, which indicates that the number of interactions is not as important as intrinsic nature and strength, type of interaction, and donor role. Although the number of IMHBs is not a primary stabilizing factor, a cooperative effect exists among IMHB networks with varying influence on the interactions individually. For example, the structure of εII_a was modified to prevent $OH\cdots N_\alpha$ by rotating the OH bond away from NH_2, resulting in significant lengthening and weakening of the remaining two IMHBs, $C_\beta H\cdots O$ and $N_\alpha H\cdots N_\delta$ by 0.151 Å, 0.068 mdyn/Å and 0.267 Å, 0.075 mdyn/Å, respectively. Conversely, eliminating $N_\alpha H\cdots N_\delta$ by flipping the Im-ring and protonating N_δ instead of N_ε resulted in a much smaller change to $OH\cdots N_\alpha$ (+0.060 Å, −0.019 mdyn/Å) and $C_\beta H\cdots O$ is shortened (−0.103 Å) and strengthened (+0.016 mdyn/Å). Optimizing the aforementioned structure also results in the Im ring flipping back to its original orientation, thus allowing for re-introduction of the $N_\alpha H\cdots N_\delta$ interaction. Another attempt to remove $N_\alpha H\cdots N_\delta$ was executed by rotating the $C_\alpha - C_\beta$ bond ≈ 180°, so H_α is forward-facing. This approach, however, leads to a

Table 2 Relative electronic plus zero-point energies (ΔE), electronic plus thermal enthalpies (ΔH), electronic plus thermal free energies (ΔG), CCSD(T) ΔE corrections (ΔE_{corr}), IMHB distances (r), local stretching force constants (k^a), and local mode frequencies (ω^a) of neutral and zwitterionic form of the most stable conformer in solution (water)

Conformer	ΔE	ΔH	ΔG	ΔE_{corr}	Parameter	r	k^a	ω^a
Neutral	0.51	0.17	0.65	3.55	$N_\alpha - H\cdots N_\delta$	2.174	0.110	446
					$O - H\cdots N_\alpha$	1.788	0.248	669
					$O\cdots H\text{-}C_\beta H$	2.687	0.135	491
Zwitter	0.00	0.00	0.00	0.00	$N_\alpha - H\cdots N_\delta$	1.856	0.208	612
					$O\text{-}H\cdots N_\alpha$	1.015	6.864	3520
					$O\cdots H - C_\beta H$	2.637	0.130	483

Calculated at B3LYP-D3(BJ)/aug-cc-pVTZ//DLPNO-CCSD(T)/aug-cc-pVTZ levels of theory. The solvent effect was calculated using PCM model. Thermochemical data are reported as relative to zwitterionic form in kcal/mol, r in Å, k^a in mdyn/Å, and ω^a in cm^{-1}

transition state. Based on this example, $OH\cdots N_\alpha$ strengthens the IMHB network, whereas $N_\alpha H\cdots N_\delta$ and $C_\beta H\cdots O$ do so to a lesser degree, or not at all.

Depending on physiological properties such as pH and temperature, histidine exists in two different forms: a neutral and a zwitterionic form [4]. Our results show that the latter form is more favorable in water by 3.55 kcal/mol compared to the former (see Table 2). In water, the $O - H\cdots N_\alpha$ (type 6) found in the zwitterionic form is by far stronger than the one found in the neutral form parallel to the thermodynamic results (see Table 2). The zwitterionic form is known to be more dominant in the solution as a result of gaining extra stabilization energy through interactions with the polar environment [10]. In the gas phase, the neutral form is more favorable compared to the zwitterionic form. However, neutral HIS has proven difficult to isolate and characterize experimentally due to its high melting point, low vapor pressure, and thermal instability [12, 13].

4 Conclusions

In this work for the first time, we quantified IMHB strength in neutral HIS and established a link between this property and structural stability/conformational preferences. Increase in bond strength and covalent properties correlate with increase in thermochemical stability. $O - H\cdots N_\alpha$ (type 6) is the IMHB having the largest effect on structural stability due to increased bond strength, covalent character, and low susceptibility to cooperative effects. We also found donor/acceptor identity to play a major role in conformational stability, and not the number of IMHBs. Details of our major findings are summarized as follows:

1. Strength of the IMHB (BSO n, k^a, and $\rho(\mathbf{r}_b)$):

   $O - H\cdots N_\alpha >> HO/O\cdots H\text{-}C_\beta H > N_\delta/O\cdots H\text{-}N_\alpha H > N_\delta - H\cdots N_\alpha >> N_\delta - H\cdots O > HC_\delta\cdots H\text{-}N_\alpha H$

2. Donor ability to increase BSO n: $H - O > H - C_\beta > H - N_\alpha > H - N_\delta$; acceptor plays a lesser role
3. Cumulative strength of IMHB networks correlates with ΔE:

   $\varepsilon II_a > \delta II_a > \varepsilon II_a > \delta I_a$

4. Observed donor–acceptor roles: CH_2 is a surprisingly capable donor, OH is a superior donor due to its polar nature, NH_2 and Im are surprisingly poor donors, and any combination of NH_2 donor/acceptor and Im donor/acceptor results in the weakest IMHBS

Future goals are to complete a comprehensive analysis of molecules capable of $N_\alpha - H\cdots C_\delta$, $C_\beta - H\cdots OH$, $C_\beta - H\cdots O{=}C$, and other HBs involving carbon to determine their similarities/differences between more well-studied and traditional HBs. The local mode analysis will play a key role because it provides a unique and quantitative measure of the intrinsic strength of a HB and any other weak chemical interaction or chemical bond.

Acknowledgements This work was financially supported by the National Science Foundation, Grant CHE 1464906. The authors thank SMU HPC for providing generous computational resources.

Compliance with ethical standards

Conflict of interest The authors declare that they have no conflict of interest.

References

1. Kulis-Horn RK, Persicke M, Kalinowski J (2013) Histidine biosynthesis, its regulation and biotechnological application incorynebacterium glutamicum. Microb Biotechnol 7(1):5–25. https://doi.org/10.1111/1751-7915.12055
2. Xue SF, Lu LF, Wang QX, Zhang S, Zhang M, Shi G (2016) An integrated logic system for time-resolved fluorescent "turn-on" detection of cysteine and histidine base on terbium (iii) coordination polymer-copper (ii) ensemble. Talanta 158:208–213. https://doi.org/10.1016/j.talanta.2016.05.066
3. Yadav K, Rao JL, Srinivas R, Nagaraj R, Jagannadham M (2018) Characterization of acetylated histidine b1-ion structure: a competition between oxazolone and side chain imidazole moiety. Eur J Mass Spectrom 24(3):261–268. https://doi.org/10.1177/1469066718756801
4. Nelson DL, Cox MM (2009) Lehninger biochemie. Springer, Berlin
5. Rebek J (1990) On the structure of histidine and its role in enzyme active sites. Struct Chem 1(1):129–131. https://doi.org/10.1007/bf00675792
6. Desfrançois C, Carles S, Schermann JP (2000) Weakly bound clusters of biological interest. Chem Rev 100(11):3943–3962. https://doi.org/10.1021/cr990061j
7. Biswal HS, Wategaonkar S (2009) Nature of the N-H ⋯ S Hydrogen Bond. J Phys Chem A 113(46):12763–12773. https://doi.org/10.1021/jp907658w
8. Lee SS, Kim JY, Han Y, Shim HJ, Lee S (2015) Thermodynamic and Kinetic Stability of Zwitterionic Histidine: Effects of Gas Phase Hydration. Chem Phys Lett 637:42–50. https://doi.org/10.1016/j.cplett.2015.08.003
9. Purushotham U, Zipse H, Sastry GN (2016) A first-principles investigation of histidine and its ionic counterparts. Theor Chem Acc. https://doi.org/10.1007/s00214-016-1926-5
10. Braga CB, Rittner R (2017) Combined utilization of 1H NMR, IR, and theoretical calculations to elucidate the conformational preferences of some L-histidine derivatives. J Phys Chem A 121(3):729–740. https://doi.org/10.1021/acs.jpca.6b12515
11. Hernández B, Pflüger F, Adenier A, Kruglik SG, Ghomi M (2010) Vibrational analysis of amino acids and short peptides in hydrated media. VIII. Amino acids with aromatic side chains: L-Phenylalanine, L-Tyrosine, and L-Tryptophan. J Phys Chem B 114(46):15319–15330. https://doi.org/10.1021/jp106786j
12. Huang Z, Yu W, Lin Z (2006) First-principle studies of gaseous aromatic amino acid histidine. J Mol Struc: THEOCHEM 801(1–3):7–20. https://doi.org/10.1016/j.theochem.2006.08.053
13. Huang Z, Lin Z, Song C (2007) Protonation processes and electronic spectra of histidine and related ions. J Phys Chem A 111(20):4340–4352. https://doi.org/10.1021/jp067280a
14. Bermúdez C, Mata S, Cabezas C, Alonso JL (2014) Tautomerism in neutral histidine. Angew Chem Int Ed 53(41):11015–11018. https://doi.org/10.1002/anie.201405347
15. Wilson EB, Decius JC, Cross PC (1955) Molecular vibrations. McGraw-Hill, New York
16. Woodward LA (1972) Introduction to the theory of molecular vibrations and vibrational spectroscopy. Oxford University Press, Oxford
17. Herzberg G (1991) Molecular spectra and molecular structure. infrared and raman spectra of polyatomic molecules, vol II. Krieger Publishing Co, New York
18. Herzberg G, Huber KP (1979) Molecular spectra and molecular structure IV. Constants of diatomic molecules. Van Nostrand, Reinhold, New York
19. Cremer D, Kraka E (2010) From molecular vibrations to bonding, chemical reactions, and reaction mechanism. Curr Org Chem 14:1524–1560
20. Konkoli Z, Cremer D (1998a) A new way of analyzing vibrational spectra. I. Derivation of adiabatic internal modes. Int J Quant Chem 67(1):1–9
21. Konkoli Z, Larsson JA, Cremer D (1998a) A new way of analyzing vibrational spectra II Comparison of internal mode frequencies. Int J Quant Chem 67(1):11–27
22. Konkoli Z, Cremer D (1998b) A new way of analyzing vibrational spectra III Characterization of normal vibrational modes in terms of internal vibrational modes. Int J Quant Chem 67(1):29–40
23. Konkoli Z, Larsson JA, Cremer D (1998b) A new way of analyzing vibrational spectra. IV. Application and testing of adiabatic modes within the concept of the characterization of normal modes. Int J Quant Chem 67(1):41–55
24. Cremer D, Larsson JA, Kraka E (1998) New developments in the analysis of vibrational spectra on the use of adiabatic internal vibrational modes. In: Parkanyi C (ed) Theoretical and computational chemistry, Elsevier, Amsterdam, pp 259–327. https://doi.org/10.1016/s1380-7323(98)80012-5
25. Zou W, Kalescky R, Kraka E, Cremer D (2012) Relating normal vibrational modes to local vibrational modes with the help of an adiabatic connection scheme. J Chem Phys 137(8):084114. https://doi.org/10.1063/1.4747339
26. Zou W, Cremer D (2016) C_2 in a Box: determining its intrinsic bond strength for the $X^1\Sigma_g^+$ ground state. Chem Eur J 22:4087–4097
27. Kraka E, Larsson JA, Cremer D (2010) Generalization of the badger rule based on the use of adiabatic vibrational modes. In: Grunenberg J (ed) Computational spectroscopy, Wiley, New York, pp 105–149. https://doi.org/10.1002/9783527633272.ch4
28. Kalescky R, Kraka E, Cremer D (2013a) Identification of the strongest bonds in chemistry. J Phys Chem A 117(36):8981–8995. https://doi.org/10.1021/jp406200w
29. Kraka E, Cremer D (2009) Characterization of CF bonds with multiple-bond character: bond lengths, stretching force constants, and bond dissociation energies. ChemPhysChem 10(4):686–698. https://doi.org/10.1002/cphc.200800699
30. Kraka E, Setiawan D, Cremer D (2015) Re-evaluation of the bond length-bond strength rule: the stronger bond is not always the shorter bond. J Comp Chem 37(1):130–142. https://doi.org/10.1002/jcc.24207
31. Setiawan D, Sethio D, Cremer D, Kraka E (2018) From strong to weak NF bonds: on the design of a new class of fluorinating agents. Phys Chem Chem Phys 20(37):23913–23927. https://doi.org/10.1039/c8cp03843k
32. Sethio D, Daku LML, Hagemann H, Kraka E (2019) Quantitative assessment of B-B-B , $B\text{-}H_b-B$, and $B\text{-}H_t$ bonds: from BH3 to $B12H12^{2-}$. ChemPhysChem. https://doi.org/10.1002/cphc.201900364
33. Oliveira V, Kraka E, Cremer D (2016a) The intrinsic strength of the halogen bond: electrostatic and covalent contributions described by coupled cluster theory. Phys Chem Chem Phys 18(48):33031–33046. https://doi.org/10.1039/c6cp06613e
34. Oliveira V, Kraka E, Cremer D (2016b) Quantitative assessment of halogen bonding utilizing vibrational spectroscopy. Inorg Chem 56(1):488–502. https://doi.org/10.1021/acs.inorgchem.6b02358
35. Oliveira V, Cremer D (2017) Transition from metal-ligand bonding to halogen bonding involving a metal as halogen acceptor: a study of Cu, Ag, Au, Pt, and Hg complexes. Chem Phys Lett 681:56–63. https://doi.org/10.1016/j.cplett.2017.05.045
36. Yannacone S, Oliveira V, Verma N, Kraka E (2019) A continuum from halogen bonds to covalent bonds: where do λ^3 Iodanes fit? Inorganics 7(4):47. https://doi.org/10.3390/inorganics7040047

37. Oliveira V, Cremer D, Kraka E (2017) The many facets of chalcogen bonding: described by vibrational spectroscopy. J Phys Chem A 121(36):6845–6862. https://doi.org/10.1021/acs.jpca.7b06479
38. Oliveira V, Kraka E (2017) Systematic coupled cluster study of noncovalent interactions involving halogens, chalcogens, and pnicogens. J Phys Chem A 121(49):9544–9556. https://doi.org/10.1021/acs.jpca.7b10196
39. Setiawan D, Kraka E, Cremer D (2015) Hidden bond anomalies: the peculiar case of the fluorinated amine chalcogenides. J Phys Chem A 119(36):9541–9556. https://doi.org/10.1021/acs.jpca.5b05157
40. Setiawan D, Kraka E, Cremer D (2014a) Strength of the pnicogen bond in complexes involving group va elements N, P, and As. J Phys Chem A 119(9):1642–1656. https://doi.org/10.1021/jp508270g
41. Setiawan D, Kraka E, Cremer D (2014b) Description of pnicogen bonding with the help of vibrational spectroscopy-the missing link between theory and experiment. Chem Phys Lett 614:136–142. https://doi.org/10.1016/j.cplett.2014.09.030
42. Setiawan D, Cremer D (2016) Super-pnicogen bonding in the radical anion of the fluorophosphine dimer. Chem Phys Lett 662:182–187. https://doi.org/10.1016/j.cplett.2016.09.028
43. Sethio D, Oliveira V, Kraka E (2018) Quantitative assessment of tetrel bonding utilizing vibrational spectroscopy. Molecules 23(11):2763. https://doi.org/10.3390/molecules23112763
44. Freindorf M, Kraka E, Cremer D (2012) A comprehensive analysis of hydrogen bond interactions based on local vibrational modes. Int J Quant Chem 112(19):3174–3187. https://doi.org/10.1002/qua.24118
45. Kalescky R, Zou W, Kraka E, Cremer D (2012) Local vibrational modes of the water dimer–comparison of theory and experiment. Chem Phys Lett 554:243–247. https://doi.org/10.1016/j.cplett.2012.10.047
46. Kalescky R, Kraka E, Cremer D (2013b) Local vibrational modes of the formic acid dimer - the strength of the double H-bond. Mol Phys 111(9–11):1497–1510. https://doi.org/10.1080/00268976.2013.796070
47. Tao Y, Zou W, Jia J, Li W, Cremer D (2016) Different ways of hydrogen bonding in water - why does warm water freeze faster than cold water? J Chem Theory Comput 13(1):55–76. https://doi.org/10.1021/acs.jctc.6b00735
48. Tao Y, Zou W, Kraka E (2017) Strengthening of hydrogen bonding with the push-pull effect. Chem Phys Lett 685:251–258. https://doi.org/10.1016/j.cplett.2017.07.065
49. Makoś MZ, Freindorf M, Sethio D, Kraka E (2019) New insights into Fe-H $_2$ and Fe-H $^-$ bonding of a [NiFe] hydrogenase Mmmic–a local vibrational mode study. Theor Chem Acc 138(6):76. https://doi.org/10.1007/s00214-019-2463-9
50. Lyu S, Beiranvand N, Freindorf M, Kraka E (2019) Interplay of ring puckering and hydrogen bonding in deoxyribonucleosides. J Phys Chem A 123:7087–7103
51. Humason A, Zou W, Cremer D (2014) 11,11-Dimethyl-1,6-methano[10]annulene-An annulene with an ultralong CC bond or a fluxional molecule? J Phys Chem A 119(9):1666–1682. https://doi.org/10.1021/jp5082966
52. Badger RM (1934) A relation between internuclear distances and bond force constants. J Chem Phys 2:128–131
53. Cremer D, Kraka E (1984a) Chemical bonds without bonding electron density? Does the difference electron-density analysis suffice for a description of the chemical bond? Angew Chem Int Ed 23(8):627–628. https://doi.org/10.1002/anie.198406271
54. Cremer D, Kraka E (1984b) A description of the chemical bond in terms of local properties of electron density and energy. Croatica Chem Acta 57:1259–1281
55. Bader R (1994) Atoms in molecules: a quantum theory. Oxford University Press, Oxford
56. Bader R (1998) Atoms in Molecules. Chem Rev 1:64
57. Grimme S (2006) Semiempirical GGA-type density functional constructed with a long-range dispersion correction. J Comput Chem 27(15):1787–1799. https://doi.org/10.1002/jcc.20495
58. Grimme S, Antony J, Ehrlich S, Krieg H (2010) A consistent and accurate ab initio parametrization of density functional dispersion correction (DFT-D) for the 94 elements H-Pu. J Chem Phys 132(15):154104. https://doi.org/10.1063/1.3382344
59. Grimme S, Ehrlich S, Goerigk L (2011) Effect of the damping function in dispersion corrected density functional theory. J Comput Chem 32(7):1456–1465. https://doi.org/10.1002/jcc.21759
60. Becke AD (1993) Density-functional thermochemistry. III. The role of exact exchange. J Chem Phys 98(7):5648–5652. https://doi.org/10.1063/1.464913
61. Chai JD, Head-Gordon M (2008) Long-range corrected hybrid density functionals with damped atom-atom dispersion corrections. Phys Chem Chem Phys 10(44):6615. https://doi.org/10.1039/b810189b
62. Krishnan R, Binkley JS, Seeger R, Pople JA (1980) Self-consistent molecular orbital methods. XX. A basis set for correlated wave functions. J Chem Phys 72(1):650–654. https://doi.org/10.1063/1.438955
63. Dunning TH (1989) Gaussian basis sets for use in correlated molecular calculations. I. The atoms boron through neon and hydrogen. J Chem Phys 90(2):1007–1023. https://doi.org/10.1063/1.456153
64. Woon DE, Dunning TH (1994) Gaussian basis sets for use in correlated molecular calculations. IV. Calculation of static electrical response properties. J Chem Phys 100(4):2975–2988. https://doi.org/10.1063/1.466439
65. Riplinger C, Neese F (2013) An efficient and near linear scaling pair natural orbital based local coupled cluster method. J Chem Phys 138(3):034106. https://doi.org/10.1063/1.4773581
66. Riplinger C, Sandhoefer B, Hansen A, Neese F (2013) Natural triple excitations in local coupled cluster calculations with pair natural orbitals. J Chem Phys 139(13):134101. https://doi.org/10.1063/1.4821834
67. Frisch MJ, Trucks GW, Schlegel HB, Scuseria GE, Robb MA, Cheeseman JR, Scalmani G, Barone V, Mennucci B, Petersson GA, Nakatsuji H, Caricato M, Li X, Hratchian HP, Izmaylov AF, Bloino J, Zheng G, Sonnenberg JL, Hada M, Ehara M, Toyota K, Fukuda R, Hasegawa J, Ishida M, Nakajima T, Honda Y, Kitao O, Nakai H, Vreven T, Montgomery JA Jr, Peralta JE, Ogliaro F, Bearpark M, Heyd JJ, Brothers E, Kudin KN, Staroverov VN, Kobayashi R, Normand J, Raghavachari K, Rendell A, Burant JC, Iyengar SS, Tomasi J, Cossi M, Rega N, Millam JM, Klene M, Knox JE, Cross JB, Bakken V, Adamo C, Jaramillo J, Gomperts R, Stratmann RE, Yazyev O, Austin AJ, Cammi R, Pomelli C, Ochterski JW, Martin RL, Morokuma K, Zakrzewski VG, Voth GA, Salvador P, Dannenberg JJ, Dapprich S, Daniels AD, Farkas Ö, Foresman JB, Ortiz JV, Cioslowski J, Fox DJ (2016) Gaussian09 revision D.01. Gaussian Inc, Wallingford CT
68. Neese F (2011) The ORCA program system. WIREs Comput Mol Sci 2(1):73–78. https://doi.org/10.1002/wcms.81
69. Weinhold F, Landis CR (2003) Valency and bonding: a natural bond orbital donor-acceptor perspective. Cambridge University Press, Cambridge
70. Reed AE, Curtiss LA, Weinhold F (1988) Intermolecular interactions from a natural bond orbital. Donor-acceptor viewpoint. Chem Rev 88(6):899–926. https://doi.org/10.1021/cr00088a005
71. Kraka E, Filatov M, Zou W, Grafenstein J, Izotov D, Gauss J, He Y, Wu A, Polo V, Olsson L, Konkoli Z, He Z, Cremer D (2017) COLOGNE2017. Southern Methodist University, Dallas, TX
72. Bader RFW (1991) A quantum theory of molecular structure and its applications. Chem Rev 91(5):893–928. https://doi.org/10.1021/cr00005a013

73. Keith TA (2017) AIMAll (Version 17.11.14). (aimtkgristmillcom)
74. Pettersen EF, Goddard TD, Huang CC, Couch GS, Greenblatt DM, Meng EC, Ferrin TE (2004) UCSF chimera? A visualization system for exploratory research and analysis. J Comput Chem 25(13):1605–1612. https://doi.org/10.1002/jcc.20084
75. Contreras-García J, Johnson ER, Keinan S, Chaudret R, Piquemal JP, Beratan DN, Yang W (2011) NCIPLOT: a program for plotting noncovalent interaction regions. J Chem Theory Comput 7(3):625–632. https://doi.org/10.1021/ct100641a
76. Johnson ER, Keinan S, Mori-Sánchez P, Contreras-García J, Cohen AJ, Yang W (2010) Revealing noncovalent interactions. J Am Chem Soc 132(18):6498–6506. https://doi.org/10.1021/ja100936w
77. de Silva P, Corminboeuf C (2014) Simultaneous visualization of covalent and noncovalent interactions using regions of density overlap. J Chem Theory Comput 10(9):3745–3756. https://doi.org/10.1021/ct500490b
78. Espinosa E, Alkorta I, Elguero J, Molins E (2002) From weak to strong interactions: a comprehensive analysis of the topological and energetic properties of the electron density distribution involving X-H ··· F-Y systems. J Chem Phys 117(12):5529–5542. https://doi.org/10.1063/1.1501133
79. Amini S, Hadipour N, Elmi F (2004) A study of hydrogen bond of imidazole and its 4-nitro derivative by ab initio and DFT calculated NQR parameters. Chem Phys Lett 391(1–3):95–100. https://doi.org/10.1016/j.cplett.2004.04.065
80. Steiner T, Desiraju GR (1998) Distinction between the weak hydrogen bond and the van der waals interaction. Chem Commun 8:891–892. https://doi.org/10.1039/a708099i
81. Steiner T (1997) Unrolling the hydrogen bond properties of C-H ··· O interactions. Chem Commun 8:727–734. https://doi.org/10.1039/a603049a
82. Desiraju GR (1996) The C-H ··· O hydrogen bond: Structural implications and supramolecular design. Acc Chem Res 29(9):441–449. https://doi.org/10.1021/ar950135n
83. Krimm S, Kuroiwa K (1968) Low temperature infrared spectra of polyglycines and C-H ··· O = C hydrogen bonding in polyglycine II. Biopolymers 6(3):401–407. https://doi.org/10.1002/bip.1968.360060311
84. Berkovitch-Yellin Z, Leiserowitz L (1984) The role played by C-H ··· O and C-H ··· N interactions in determining molecular packing and conformation. Acta Crystallogr B 40(2):159–165. https://doi.org/10.1107/s0108768184001919
85. Kovačević B, Rožman M, Klasinc L, Srzić D, Maksić ZB, Yáñez M (2005) Gas-phase structure of protonated histidine and histidine methyl ester: combined experimental mass spectrometry and theoretical ab initio study. J Phys Chem A 109(37):8329–8335. https://doi.org/10.1021/jp053288t